UVA and UVB light emitting diodes with AlyGa1-yN quantum dot active regions covering the 305-335 nm range

Julien Brault, M. Al Khalfioui, Samuel Matta, B. Damilano, Mathieu Leroux, Stéphane Chenot, Maxim Korytov, J. E. Nkek, P Vennegues, Jean-Yves Duboz, et al.

UVA and UVB light emitting diodes with $Al_yGa_{1-y}N$ quantum dot active regions covering the 305 nm – 335 nm range

J. Brault,[1,2] M. Al Khalfioui,[1,3] S. Matta,[1,4] B. Damilano,[1] M. Leroux,[1] S. Chenot,[1] M. Korytov,[1] J. E. Nkeck,[1] P. Vennéguès,[1] J. –Y. Duboz,[1] J. Massies,[1] and B. Gil[4]

[1] Université Côte d'Azur, CNRS, CRHEA, 06560 Valbonne, France

[4] CNRS-Université Montpellier 2, L2C, UMR 5221, 34095 Montpellier, France

Abstract

Ultra-violet (UV) light emitting diodes (LEDs) using III-N quantum dot (QD) active regions have been fabricated by molecular beam epitaxy on (0001)-oriented sapphire substrates. By using the epitaxial compressive stress between the QD material and the template/barrier layers, leading to a 2D-3D growth mode transition, self-assembled $Al_yGa_{1-y}N$ QDs with a nominal Al composition of 10% and 20% have been fabricated on $Al_{0.6}Ga_{0.4}N$. Atomic force microscopy and transmission electron microscopy measurements show high QD densities, ranging between $2x10^{11}$ - $5x10^{11}$ cm^{-2}, and height and diameter distributions between 1.5 - 3 nm and 5 - 20 nm. LED structures including two different $Al_yGa_{1-y}N$ / $Al_{0.6}Ga_{0.4}N$ (0001) QD active regions have then been fabricated and processed using a standard planar geometry and squared mesa structures. Current-voltage characteristics and electroluminescence (EL) measurements have been performed at room temperature. In particular, the EL properties are investigated in terms of spectral range and wavelength shift as a function of the injection current density. Typically, an emission between 325 nm – 335 nm is obtained for $Al_{0.1}Ga_{0.9}N$ QDs and between 305 nm – 320 nm for $Al_{0.2}Ga_{0.8}N$ QDs. The LED characteristics (EL wavelength and broadening) are then correlated to the QD structural properties and the results, supported by calculations, show the main influence of the QD height dispersion and composition fluctuations. Finally, the light output intensity variation as a function of the

[2] E-mail: Julien.Brault@crhea.cnrs.fr;
[3] E-mail: Mohamed.Al-Khalfioui@crhea.cnrs.fr;

injection current density has also been investigated and is discussed in terms of injection and recombination mechanisms in the devices.

Introduction

An intense research activity in nitride materials is currently dedicated to the improvement of ultra-violet (UV) light emitting diode (LED) efficiencies in the UVB and UVC ranges [1], since these wavelength spectral ranges match with an important panel of applications: e.g. UV curing, medical phototherapy, sterilisation or water and air purification [2,3]. Indeed, whereas indium gallium nitride (In,Ga)N based blue LEDs reach external quantum efficiencies (EQE) above 80% [4], the necessity to use aluminium gallium nitride ($Al_xGa_{1-x}N$) materials in order to shift the emission into the UV range leads to a strong decrease in the EQE, which is typically below 10%. A low EQE, which is defined as the product of the injection efficiency (IE) times the radiative efficiency (RE) and the extraction efficiency (EE), accounts for either poor electrical characteristics, reduced material quality, low photon extraction or a combination of these parameters. In particular, standard growth processes of $Al_xGa_{1-x}N$ layers by molecular beam epitaxy (MBE) or metal organic vapor phase epitaxy on sapphire substrates lead to very high dislocation densities (DDs) (in the 10^{10} - 10^{11} cm^{-2} range), which are detrimental to the RE of active regions [5]. In fact, compared to the GaN/(In,Ga)N system, a much stronger impact of dislocations on the quantum well (QW) RE in the (Al,Ga)N/(Al)GaN system is found and attributed, at least partly, to a weaker in-plane spatial localization of excitons than is typically observed in (In,Ga)N QWs [6]. To reduce the DDs in $Al_xGa_{1-x}N$ layers, epitaxial processes such as the lateral overgrowth method [7], patterned or thermally decomposed sapphire surface [8,9], high temperature annealing [10,11] are being developed, leading to important reduction of DDs down to the 10^8 cm^{-2} range. Another possibility is to increase the spatial localization of excitons by fabricating three dimensional (3D) confining potentials, i.e. by using $Al_yGa_{1-y}N$ potential fluctuations [12 , 13] or nanostructures such as quantum dots (QDs) [14,15], which have been shown to efficiently decrease non radiative channels and lead to high RE up to room temperature [16,17]. A way

to fabricate QDs is to take advantage of the Stranski-Krastanov (2D-3D) growth mode which can be obtained by using compressively strained $Al_yGa_{1-y}N$ layers deposited on $Al_xGa_{1-x}N$ templates [18]. Furthermore, their formation can be followed in situ by reflection of high-energy electron diffraction (RHEED) in MBE [14,15], enabling to investigate the influence of growth conditions on the $Al_yGa_{1-y}N$ QD formation process [19].

LED structures made of $Al_yGa_{1-y}N$ QWs with potential fluctuations or GaN QDs as active regions were reported by several groups [20,21,22], demonstrating their potential for UV sources. In our case, based on the possibility to grow GaN QDs on low Al content (0001)-oriented "polar" $Al_xGa_{1-x}N$ layers [23], we have fabricated LEDs emitting in the near-UV (between 400 nm and 380 nm [24],[25]). Next, by reducing the QD size or taking advantage of the possibility to grow $(11\bar{2}2)$-oriented "semipolar" QDs [26], a shift towards shorter wavelengths was obtained, enabling to get an emission down to 360 nm for "polar" LEDs and down to 325 nm for "semipolar" ones [27]. Another approach is to grow "polar" $Al_yGa_{1-y}N$ QDs on $Al_xGa_{1-x}N$ (with $x > y$), for which we have shown the possibility to get an emission down to the UVB range at 314 nm by using QDs with a nominal Al content of 10% [18]. In this work, we propose the use of such QDs as the active regions of UV LEDs. After the investigation of $Al_yGa_{1-y}N$ QDs structural properties (with nominal Al contents of 0.1 and 0.2), we present the main electrical and optical properties of $Al_yGa_{1-y}N$ QD based LEDs. In particular, since the energy level quantization can be neglected along the $Al_yGa_{1-y}N$ QD in-plane directions, as discussed in the following sections, the investigated LED active regions should be considered as segments of quantum wells with nm-sized lateral extensions inducing 3D carrier localizations. The main emission characteristics, i.e. the EL spectral range and broadening, as well as the emitted wavelength dependence as a function of the current density is presented and discussed, in terms of QD structural properties, in correlation with

calculations. A study of the light output variation is also shown, giving insights on the carrier recombination mechanisms in these LEDs.

1. Fabrication of the quantum dot based light emitting diodes

1.1. Growth conditions of $Al_yGa_{1-y}N$ quantum dots

The structures were fabricated on the (0001) orientation of sapphire substrates by MBE in a RIBER 32 P reactor. The layers were grown using solid Al and Ga sources for III-elements, solid Si and Mg sources for n-type and p-type dopants, respectively, and NH_3 as nitrogen precursor except for the fabrication of the QDs for which a RIBER RF N_2 plasma source was used. For all the structures, a 100-nm AlN layer was first deposited at 950°C on a low temperature GaN buffer layer. Then, a 0.8-µm thick $Al_{0.6}Ga_{0.4}N$ layer was grown at 860°C, n.i.d or Si-doped for the purpose of fabricating and characterizing $Al_yGa_{1-y}N$ QDs or QD based LEDs, respectively. Therefore, a first series of samples (described in the following part) was grown to investigate the formation and the morphological properties of the QDs and a second series of samples (described in section 1.3) was dedicated to the fabrication of LED structures including a QD active region.

$Al_yGa_{1-y}N$ QDs, with an Al nominal concentration (n.c.) of 0.1 and 0.2, were spontaneously formed on $Al_{0.6}Ga_{0.4}N$ (0001) following a 2D - 3D "Stranski-Krastanov" growth mode of the $Al_yGa_{1-y}N$ layer [14,17]. This 2D – 3D transition results from the epitaxial stress caused by the in-plane lattice parameter difference between $Al_yGa_{1-y}N$ and $Al_{0.6}Ga_{0.4}N$ leading to a lattice-mismatch of 1.2% and 1% for $Al_{0.1}Ga_{0.9}N$ (n.c.) and $Al_{0.2}Ga_{0.8}N$ (n.c.) QDs, respectively, and a critical thickness $h_{2D\text{-}3D}$ ranging between 3 and 4 monolayers (MLs), with 1 ML corresponding to half the c lattice parameter, i.e. close to 0.26 nm. QDs were grown by depositing $Al_yGa_{1-y}N$ amounts between 8 and 10 MLs, under N-rich conditions with a III/V flux ratio of 0.7, a growth rate about 0.1 – 0.3 ML/s and a growth temperature of 730°C ± 10 °C. In order to improve the QD shape uniformity, a post-growth annealing process was

developed after the $Al_yGa_{1-y}N$ deposition, involving an annealing under vacuum for 6 minutes and a progressive increase of the surface temperature up to 820°C ± 10 °C, similarly to the procedure presented in ref. 19. The QD layer was then capped with a 30 nm thick $Al_{0.6}Ga_{0.4}N$ layer followed by the growth of the second uncapped QD layer. After the growth, the samples were then quickly cooled down under vacuum before being taken out of the MBE chamber.

1.2. Structural properties

The fabrication of the QDs was followed in-situ by RHEED through: i) the modification of the diffraction pattern, i.e. going from streaky to spotty as the layer undergoes a change from a 2D to a 3D morphology [28], and ii) the variation of the specular and Bragg spots intensities, as shown in figure 1(a). In this figure, three specific features in the RHEED intensity can be noticed: 1) the presence of oscillations at the first stages of the $Al_yGa_{1-y}N$ layer growth, corresponding to the initial 2D growth mode; followed by 2) an abrupt increase of the intensity corresponding to the growth mode transition from a 2D layer to 3D islands; and finally 3) a second increase of the intensity during the annealing process related to the 3D island shape transition from elongated to isotropic QDs [19]. After the growth, the morphology of the QDs at the surface was investigated by ex-situ atomic force microscopy (AFM) operating in tapping mode. Typical images of $Al_{0.1}Ga_{0.9}N$ (n.c.) and $Al_{0.2}Ga_{0.8}N$ (n.c.) QDs are presented in figure 1(b)) and (c), respectively. High QD densities are observed, between 2 x 10^{11} cm^{-2} and 5 x 10^{11} cm^{-2} with a tendency to get larger densities in the case of $Al_{0.2}Ga_{0.8}N$ (n.c.) QDs for identical deposited amounts. This feature is ascribed to the reduced surface mobility of Al adatoms compared to Ga ones, which leads to an increase of the QD nucleation center density and consequently to higher QD densities as the Al concentration in the QDs increases, as seen in the case of $Al_{0.1}Ga_{0.9}N$ (n.c.) QDs compared to GaN QDs [18,19]. The QD diameters were found between 10 nm and 20 nm, and the QD heights between 1 nm and 2.5 nm, with a tendency to get smaller QDs in both height and lateral

dimensions in the case of $Al_{0.1}Ga_{0.9}N$ (n.c.) QDs for identical deposited amounts. However, it is known that the similar dimensions of $Al_yGa_{1-y}N$ QDs and the AFM tip radius (~ 7 nm) can lead to a convolution effect that could affect the apparent shape of the QDs and an overestimation of their lateral dimensions. Therefore, in order to get more insights on the QD sizes, cross-sectional transmission electron microscopy (TEM) measurements were performed. The samples were prepared by mechanical polishing followed by ion milling. High-angle annular dark-field imaging in scanning transmission electron microscopy mode (STEM-HAADF) was performed using a JEOL 2010F microscope operating at 200 kV. Images of $Al_{0.1}Ga_{0.9}N$ (n.c.) and $Al_{0.2}Ga_{0.8}N$ (n.c.) QDs, taken along the $[11\bar{2}0]$ zone axis, are presented in figure 2(a) and 2(b), respectively. The QDs, which are composed of heavier material than the matrix, appear with a brighter contrast. For both types of QDs, similar sizes are found between 1.5 nm – 3 nm and 6 nm – 12 nm for their height and diameter, respectively, which are in fair agreement with AFM measurements although we note a tendency for smaller diameters and higher heights in TEM observations, as expected. A truncated pyramidal shape can be deduced for the QDs, with facets forming an angle of around 30° with the (0001) growth surface, which exact determination is difficult since several QDs may be present in the observed sample section forbidding any certainty to observe an isolated QD. Nevertheless, these characteristics are found to be very similar to the QD morphology found for GaN QDs [29], for which facets parallel to $\{1\bar{1}03\}$ planes have been observed, which have an inclination angle of 30° with the (0001) plane. In addition, some contrast differences can be distinguished in the capping layer, characterized by brighter regions in between two neighbouring QDs. Noteworthy, similar features have already been observed and deeply investigated in the case of GaN / $Al_xGa_{1-x}N$ QDs and found to be the consequence of a phase separation in the $Al_xGa_{1-x}N$ layer grown on top of the QD plane [29,30].

1.3. Light emitting diode design and fabrication process

Using QDs made of GaN has resulted in the fabrication of (0001) oriented LEDs emitting in the near UV range, typically between 360 nm – 400 nm [27]. Actually, the minimum wavelength values are not strictly limited by the material properties, i.e. the GaN band gap, but they are also the consequence of the strong internal electric field (F_{int}) in these "polar" structures (of the order of several MV/cm [31]), which comes from the large values of the polarization discontinuities in $Al_yGa_{1-y}N$ / $Al_xGa_{1-x}N$ (0001) heterostructures. The presence of F_{int} induces an important redshift in the emitted wavelength, typically of several tens of nm, due to the quantum confined Stark effect (QCSE). Therefore, efficient ways to reach shorter wavelengths in such heterostructures are: i) to increase the band gap energy of the QD material system, and ii) to fabricate QDs with reduced dimensions (i.e. with heights typically below 2 - 3 nm) to enhance the confinement and the quantization of energy levels and iii) to limit the influence of F_{int} on the energy level distribution. Interestingly, all these ways can be combined by using $Al_{0.1}Ga_{0.9}N$ (n.c.) QDs [19], and it can thus be expected that further increasing the Al content of the QDs will allow shifting the wavelength emission further into the UV range. Along these views, two types of $Al_yGa_{1-y}N$ / $Al_{0.6}Ga_{0.4}N$ (0001) QD-based LEDs were fabricated following identical growth conditions and structure design except for the QD Al content. For the QD active region, consisting of three QD planes, the same growth conditions as described in the previous section were used. It is worth noting that in order to follow the 2D – 3D growth mode transition by RHEED, the rotation of the samples was stopped during the growth of these layers. Therefore, the growth conditions have been chosen to yield QDs with an Al n.c. of 0.1 and 0.2 for the QDs at the center of the wafers, with $Al_{0.1}Ga_{0.9}N$ (n.c.) QD based LEDs referred as LED-A, and $Al_{0.2}Ga_{0.8}N$ (n.c.) QD based LEDs referred as LED-B. From the center to the edge of the wafers, a relative Al variation of ± 20% is estimated based on energy dispersive X-ray spectroscopy measurements performed on thick (0.5 µm) $Al_xGa_{1-x}N$ layers also fabricated without rotation of the samples: this characteristic

implies a variation of the Al n.c. of the QDs from 0.08 to 0.12 for LED-A, and from 0.16 to 0.24 for LED-B, i.e. from one side to the opposite one across the wafers. The LED structures follow the schematics presented in figure 3(a), with a Si concentration estimated in the 10^{19} cm^{-3} ranges for the n-type $Al_{0.6}Ga_{0.4}N$ layer, and an $Al_{0.6}Ga_{0.4}N$ spacer layer thickness of 10 nm between the QD planes. The $Al_yGa_{1-y}N$ QDs 2D equivalent thickness is 10 MLs (i.e. about 2.5 nm). The p-type region consists of a 20 nm $Al_{0.75}Ga_{0.25}N$:Mg electron blocking layer, a 10 nm $Al_{0.6}Ga_{0.4}N$:Mg layer and a final 30 nm thick GaN:Mg contact layer. The Mg concentrations are estimated, from previous calibration measurements by secondary ion mass spectroscopy, to be of the order of [Mg] ~ $5x10^{19}$ atoms.cm^{-3} in the $Al_xGa_{1-x}N$ layers and [Mg] ~ $1x10^{20}$ atoms.cm^{-3} in the GaN layer. After the growth, LEDs with a squared geometry were processed by using photolithography and reactive ion etching. The mesas are covered by a thin Ni / Au (5 / 5 nm) semi-transparent current spreading layer plus a Ni / Au (20 / 200 nm) contact as top electrode to p-GaN. The contact on n-$Al_{0.6}Ga_{0.4}N$ consists of a stacking of Ti / Al / Ni / Au (30 / 180 / 40 / 200 nm).

2. Light emitting diode characteristics

LEDs with a squared mesa size of 310 µm, corresponding to mesa areas of ~ 96000 $µm^2$ (and an emitting surface area about 10000 $µm^2$ less by subtracting the surface area of the n- and p-type contacts) for the light emission, have been investigated. The LEDs were characterized at room temperature by performing on wafer current - voltage (I-V) and electroluminescence (EL) measurements. The EL was measured from the backside of the LED chip by collecting the light in an UV-grade optical fiber connected to a linear CCD spectrometer with a spectral resolution of 2.5 nm.

2.1. Electrical properties

First, the current-voltage (I-V) characteristics of the devices were investigated, and no significant differences were observed between the two types of LEDs. A typical I-V curve is

presented in figure 3(b). Overall, the LEDs turn-on voltage is found around 7 (± 1) V and a value of 8.5 (± 1) V is measured at 20 mA (i.e. at a current density ~ 23 A/cm^2). The diode series resistance (R_s) values are typically found around 150 (± 50) Ω . These high values of R_s compared to GaN-based LEDs are attributed to the increase in the resistivity of doped $Al_xGa_{1-x}N$ layers for higher Al concentrations, as a strong deepening of the acceptor and donor levels occurs, in particular in the case of p-type $Al_xGa_{1-x}N$ layers [1]. The leakage current and shunt resistances have also been estimated, as can be deduced from the semi-log plot of the I-V curve in the inset of figure 3(b): the leakage current @ -4 V is found in the 50 - 100 µA range (corresponding to 0.06 – 0.12 A/cm^2) and the shunt resistance is of the order of 1 MΩ or less . The significant reverse saturation currents and low shunt resistances in the devices point out important leakage paths in the devices. Leakages in the LEDs are mainly attributed to the high density of dislocations (above 10^{10} cm^{-2}) in the structures [32].

2.2. Electroluminescence measurements

Electroluminescence (EL) measurements of different LEDs have been performed at room temperature. Due to the variation of the Al concentration in the QDs across the wafers, a shift of the EL emission in the 325 nm – 335 nm range (i.e. from 3.81 eV to 3.70 eV) and in the 305 nm – 320 nm range (i.e. from 4.06 eV to 3.88 eV) has been observed for LED-A and LED-B, respectively. As expected, an emission at higher energy is obtained for LED B, i.e. with the active region made of QDs with the larger Al nominal concentration. In the following study, we present an in-depth characterization of two typical LEDs made of $Al_{0.1}Ga_{0.9}N$ (n.c.) QDs and $Al_{0.2}Ga_{0.8}N$ (n.c.) QDs, referred as A1 and B1. The EL spectra, measured between 200 nm and 600 nm, of A1 and B1 are shown in figure 4(a) and 4(b), respectively, using an input current density of 5.7 A / cm^2 (i.e. corresponding to an injected current of 5 mA). Each spectrum is characterized by a main peak, coming from the QD emission, found at an energy of 3.80 eV (326 nm) for A1 and at a higher energy of 4.06 eV (305 nm) for B1. Yet, as

pointed out in section 1.3, the presence of an internal electric field in the QD active region could lead to a strong QCSE and a redshift of the EL emission. A way to estimate the influence of the QCSE on the QD emission is to compare the EL energy with the band gap energy of $Al_yGa_{1-y}N$ (for an Al concentration equals to 0.1 and 0.2). By using the energy band gap of $Al_yGa_{1-y}N$ alloys determined in ref. [33] and considering the strained band gap roughly estimated by using the deformation potential of GaN [34], we obtain a value of 3.72 eV and of 3.89 eV for the band gap of $Al_{0.1}Ga_{0.9}N$ and $Al_{0.2}Ga_{0.8}N$, respectively. Therefore, for both type of LEDs, the QD emission is found at a higher energy, indicating that the influence of the QCSE in the band structure is minimized, contrary to the case of GaN QD-based LEDs for which the EL emission has been observed at energies below the strained GaN band gap [24,28]. This difference is mainly attributed to the smaller QD dimensions (mainly the QD height since lateral confinement effects in nitride QDs are weak compared to those along the <0001> direction [35]) in the case of $Al_yGa_{1-y}N$ compared to GaN [19]. Indeed, for $Al_{0.1}Ga_{0.9}N/Al_{0.5}Ga_{0.5}N$ QDs, it was shown that PL energies corresponding to QD heights typically below 2.5 nm are found above the strained band gap energy of $Al_{0.1}Ga_{0.9}N$, by considering an internal electric field value of 2 ± 0.5 MV/cm [19]. Considering the EL peaks full width at half maximum (FWHM), a value of 190 meV (16 nm) has been measured for A1 whereas a value of 280 meV (22 nm) is found for B1. Noteworthy, compared to GaN-based QD-LEDs with similar mesa areas, for which EL peaks with FWHM around 350 – 400 meV were obtained [24,25], a significant reduction is observed for (Al,Ga)N-based QD-LEDs, which can also be related to the minimized influence of F_{int}, or in a more simple frame to a reduction of its value due to the decrease of polarization discontinuities, (considering that the (Al,Ga)N QD relative size (height) dispersion is similar for all types of LEDs, i.e. independent of the Al composition). However in such a case, it is worth noting that going from $Al_{0.1}Ga_{0.9}N$ (n.c.) to $Al_{0.2}Ga_{0.8}N$ (n.c.) QDs with similar $Al_xGa_{1-x}N$ barrier composition

should lead to a lower F_{int} and consequently a further reduction of the EL peak FWHM [31]. Obviously, the FWHM variation between both types of LEDs studied here indicates that F_{int} is not the only parameter accounting for the EL broadening, at least in the case of $Al_{0.2}Ga_{0.8}N$ (n.c.) QDs. A main origin can then be attributed to an increase in the QD size (height) dispersion and/or Al composition fluctuation between the QDs, when increasing the Al n.c. of $Al_yGa_{1-y}N$ QDs (along with the intrinsic alloy inhomogeneous broadening). In addition, we can note that the EL spectra show a broad emission at longer wavelengths than the main EL peak, typically in the 350 nm - 420 nm range. A similar feature has already been observed by photoluminescence in the case of $Al_{0.1}Ga_{0.9}N$ (n.c.) QDs [19] and attributed to a combination of QD height and composition fluctuations [36]. In addition, luminescence from defects below the effective band gap of the QDs or below the $Al_{0.7}Ga_{0.3}N$ band gap, which is often observed in $Al_xGa_{1-x}N$ materials, could also contribute to this broad EL band. When increasing the input current, similar EL spectra are obtained, as presented in figure 5 for a current density of 23 A / cm^2: no significant shift in the emitted wavelength is observed compared to the previous measurement with the EL peaking at 325 nm for A1 and at 305 nm for B1. However, a clear increase in the FWHM is observed, with a value of 230 meV (20 nm) and of 425 meV (32 nm) for A1 and B1, respectively. Again, an opposite behaviour was observed for the case of GaN QD-based LEDs for which the decrease of the EL peak FWHM was the result of a partial screening of F_{int} [24,25]. As discussed previously, $Al_yGa_{1-y}N$ QD-based LEDs characteristics are less influenced by F_{int} than GaN ones, and consequently, the increase of the EL peak FWHM is attributed to a broadening of the QD size and composition dispersion and/or band/state filling effects in the QDs. In particular, the use of a larger input current is expected to lead to the progressive injection of carriers into the different QD planes (in particular holes which are mainly injected into the plane next to the p-type layers at low current density due to their low mobility and concentration); therefore, the larger EL peak

FWHM would then account for a broadening of the QD size distribution from plane to plane. For instance, depending on the spacer layer thickness between the QD planes, a variation of the QD sizes has been already observed in other QD material systems, and should be potentially optimized by adjusting the spacer layer thickness [37,38].

To get more insight into these characteristics, the variations of the EL peak energy as a function of the input current density have also been investigated, as presented in figure 6(a) and 6(b) for A1 and B1, respectively. As highlighted in both figures, three different regimes can be distinguished: 1) at lower current densities (region I), a blueshift of the EL peak energy is observed when the current density increases, with the emitted wavelength varying from 331 nm to 325 nm for A1 and from 314 nm to 305 nm for B1. This shift corresponds to an energy variation of around 70 meV and 120 meV for A1 and B1, respectively. This shift is attributed to a partial screening of F_{int} and band/state filling effects by the increase of the carrier density in the QDs, as for GaN QD-based LEDs [24,25]. At this stage, it is worth noting that a similar energy shift value has been observed in the case of GaN QD based LEDs with small QD heights (i.e. typically 2 nm or less), whereas much larger energy shifts (up to 500 meV) where observed for larger (higher) GaN QDs [27]. Obviously, since F_{int} was identical in these two types of LEDs, the large reduction in the energy shift could be straightforwardly attributed to the reduced QD heights (resulting in a minimized influence of F_{int}). Actually, these results are in agreement with the previous discussion related to the QD EL energies and the associated weak influence of F_{int}. Therefore, the QD size (height) distribution is expected to be the main parameter accounting for the broadening of the EL spectra. 2) At intermediate current densities (region II), a saturation to a minimum wavelength value is obtained. This saturation is seen as the consequence of two opposite effects, which are counterbalancing each other: a (weak) screening of F_{int} together with a (weak) increase of the LED junction temperature. 3) At larger current densities (region III), an opposite behaviour compared to the one observed at

lower current densities is found, with a progressive decrease of the EL peak energy, i.e. a redshift, and an increase of the emitted wavelength from 325 nm to 330 nm and from 305 nm to 311 nm, for A1 and B1, respectively. The origin of this characteristic is associated to the high series resistance of the LEDs and mostly the high resistivity of the $Al_xGa_{1-x}N$ p-type layers, leading to an important Joule heating and an important increase of the LED junction temperature and, consequently, to a decrease of the $Al_yGa_{1-y}N$ QD band gap energy.

2.3. Calculations and EL interpretations

In order to corroborate the interpretation of our EL spectra from the LEDs, calculations have been performed with the Schrödinger-Poisson equation solver (Nextnano) in the effective mass approximation. The temperature was set at 300K. Due to their large lateral/vertical size ratio, QDs were modeled as QWs, and lateral confinement was not taken into account [35]. The QWs are supposed to be strained on the $Al_{0.4}Ga_{0.6}N$ (0001) barriers. However, in order to account for a possible partial strain relaxation in the QDs, a 50% strain relaxation in the QW was introduced in the calculation, reducing by the same amount the piezoelectric component of the electric field. The spontaneous component was not modified. As a result, the total electric field discontinuity at the QW / barrier interface reaches 4.01 MV / cm and 3.38 MV / cm for QWs with 10% and 20% respectively. Periodic conditions were taken for the potential which reasonably applies in LEDs under forward injection when flat band conditions are reached. A uniform n doping of 10^{17} cm^{-3} was taken in both the QW and barrier to mimic the residual doping. Results for the transition energies of the fundamental electron-hole recombination as a function of the QD height (i.e. QW thickness) show values in fair agreement to the EL measurements (fig. 7(a)): indeed, considering the EL energy at maximum intensity, i.e. 3.80 eV for A1 and 4.06 eV for B1, an average QD height of 1.9 nm (± 0.1 nm) can be deduced for both devices, in fair agreement with the QD structural measurements described in section 1.2. In addition, the electron-hole wave function overlap was determined

and also reported in fig. 7(a), showing as expected a strong decrease as a function of the QD height, as a consequence of the QCSE. For instance, a variation of the QW thickness from 1.5 nm to 2.5 nm leads to a decrease of the overlap from 0.5 to 0.1. We can also notice that very similar values are obtained for both types of QDs, for heights ranging between 1 nm and 2 nm. For higher QDs, larger values are obtained in the case of $Al_{0.2}Ga_{0.8}N$ / $Al_{0.6}Ga_{0.4}N$ QDs, as a consequence of the lower F_{int}, with typically an increase going from 10% to 25% for thicknesses increasing from 2 nm to 3 nm.

Taking into account the EL emission energy range corresponding to the EL peak FWHM, i.e. between 3.7 eV and 3.9 eV for A1 and between 3.75 eV and 4.2 eV for B1, a height distribution of the QD population between 1.6 nm – 2.2 nm and between 1.3 nm – 3.0 nm can be estimated for $Al_{0.1}Ga_{0.9}N$ and $Al_{0.2}Ga_{0.8}N$ QDs, respectively. Therefore, as discussed in the previous section, the broadening of the EL peaks can be associated to a strong increase of the QD height dispersion when increasing the Al concentration. Yet, this estimation is based on the consideration of a QD composition identical to the n.c., whereas some fluctuations can be expected, as reported in ref. 36. Indeed, considering a Gaussian distribution of the QD heights centred at 2 nm with a standard deviation of 0.3 nm, equivalent to a FWHM of 0.7 nm in fair agreement with experimental results obtained by AFM [36], gives an emission with a FWHM of 230 meV (fig. 7(b)) and 190 meV (fig. 7(c)) for $Al_{0.1}Ga_{0.9}N$ and $Al_{0.2}Ga_{0.8}N$ QDs, respectively. Therefore, the EL spectral broadening of A1 can be well explained by such QD height dispersion whereas a reduction of the FWHM should be observed for B1, contrary to the experimental observations. Together with height dispersion, composition fluctuations can also be present in the QD population which have also been taken into account in the second plot of fig. 7(c), considering a mean Al content of 20% and a Gaussian parameter of 2% (i.e. a variation of the Al composition from ~ 18% to 22%). In this case, the value of the FWHM of the emission is then equal to the square root of the sum of the square value of the FWHM

related to the QD height dispersion and the square value of the FWHM related to the QD composition fluctuation. A significant increase of the FWHM – from 190 meV to 225 meV – is then calculated, in closer agreement to the experimental results indicating that QD composition fluctuations have an impact, although weaker than the QD height dispersion, on the EL characteristics of B1.

3. Discussion

The dependence of the LED peak emission as a function of the input current densities has shown three distinct regimes from lower to higher injection currents, as described in section 2.2. Such behaviours and injection mechanisms into the LED active regions have been further evidenced by analyzing the light output-current (L-I) characteristics of the LEDs, i.e. by plotting the variation of the EL integrated intensity (between 280 nm and 400 nm) as a function of the injection current, as presented in figure 8. Two different types of LED designs for the n-type contact have been investigated for identical mesa area (~ 96000 μm^2), with the contact surrounding the entire mesa (figure 8(a)) or being isolated at one side of the LED mesa (figure 8(b)). Independently of the LED design, it can clearly be seen that the light output varies as a function of the input current at a constant power m, i.e. L is proportional to I^m with m values ranging from 0.09 to 2.5 for different ranges of current densities. Once again three different regimes are observed, similarly to the EL energy (wavelength) variation as a function of I described in the above section. Actually, this parameter m gives information about the recombination mechanisms involved in the LEDs [39,40]. At lower injection currents, i.e. for densities between 1 – 10 A/cm^2, a super linear dependence (m > 1) of L is observed, with a variation equal or close to the square of I, which behaviour is characteristic of LEDs dominated by non-radiative mechanisms: such mechanisms have been attributed either to tunnelling processes of carriers into defect states localized in the cladding layers or band gap states in the QD active layers. Depending on the LED design, under intermediate

injection currents, i.e. for densities between 10 – 40 A / cm^2, either a linear or an under linear variation of L is found, in figure 8(a) and (b), respectively. The linear variation case (figure 8(a)) implies that the deep-level states are saturated and the LED internal quantum efficiency (IQE) is constant. This characteristic is observed for the LED designed with the n contact surrounding the entire mesa. In the other case, m is found below 1, implying the LED output power progressively starts to saturate with the input current. This behaviour is observed for both types of LEDs at higher injection currents (above 40 A / cm^2), and it is even further enhanced with m values approaching zero, i.e. leading to an almost constant value of L independently of I. In these cases, the LED IQE is strongly decreasing. Noteworthy, this regime coincides with the redshift variation of the EL peak as a function of the injection current (figure 6), implying that important thermal effects are at stake in the junction of the LEDs: this characteristic is related to low injection efficiencies and poor current spreading. Indeed, the use of an n contact surrounding the entire mesa clearly improves the injection efficiency and current spreading, enabling to increase the light output of the LED up to larger injection current densities compared to the case of an isolated n contact at one side of the LED mesa. Obviously, from these results, it appears that the LED design and technological process need further improvements: at first, the IQEs of the QDs, estimated at around 10% from previous studies [18,19] can still be improved ; secondly, the very high dislocation densities (in the 10^{10} cm^{-2} range [23]) lead to shunt paths in the LEDs, and to important leakage currents, causing a reduction of the carrier injection into the active region. In addition, the super linear dependency of the light output at low current densities indicates important non radiative mechanisms which are directly related to the reduced material quality of our epitaxial structures, affecting the IQE. Also, an increase of the number of QD planes, and a reduction of the capping layer thickness would favor the carrier injection in the QDs as well as increase the light output; at last, thermal management should be improved, in particular for

high input current density operations, since important thermal effects have been observed, leading to a severe drop of the IE. For instance, these thermal effects could come from inefficient hole injection due to low hole concentration and mobility in high Al concentration $Al_xGa_{1-x}N$ layers leading to electron leakage and overflow out of the active region [41], requiring the development of specific p-type layer designs.

4. Conclusion

By taking advantage of a 2D-3D morphological transition during the growth of strained $Al_yGa_{1-y}N$ (0001) layers, quantum dots (QDs) have been fabricated using two different Al nominal concentrations (n.c.) of 0.1 and 0.2 on $Al_{0.6}Ga_{0.4}N$ (0001) templates. The QD shape, size and density have been studied by atomic force microscopy and transmission electron microscopy measurements, showing high densities above 10^{11} / cm^2, heights between 1.5 nm and 3 nm and diameters ranging from 5 nm to 20 nm. Next, the potential of such QDs for UV sources has been assessed by fabricated light emitting diodes (LEDs) using both types of QDs. It has been shown that $Al_{0.1}Ga_{0.9}N$ (n.c.) QDs enable to get LEDs emitting in the short wavelength side of the UVA region, between 325 nm and 335 nm, whereas $Al_{0.2}Ga_{0.8}N$ (n.c.) QDs lead to an emission close to the centre of the UVB region, between 305 nm and 320 nm. Only a limited influence of the internal electric field on the electroluminescence (EL) properties of the LEDs has been observed (compared to the former case of GaN QD-based LEDs), with a maximum EL peak energy shift limited to around 100 meV, as a consequence of the small heights of the QDs. However, despite this limited influence, wide EL peaks are observed and have been mainly attributed to the height dispersion in the QD population, in correlation with calculations. Also, an additional broadening observed for $Al_{0.2}Ga_{0.8}N$ (n.c.) QDs has been associated to a significant contribution of composition fluctuations in the QDs. As a general trend, three distinct operating regimes have been observed as a function of the input current densities strongly modifying the light output characteristics of the LEDs from

lower to larger current values. In particular, recombination mechanisms and thermal effects have been studied, pointing at the importance of the LED design on the injection efficiency and current spreading, which are seen as severe issues in $Al_xGa_{1-x}N$ based LEDs.

Acknowledgments

The authors would like to thank D. Lefebvre, S. Vézian, A. Courville and B. Poulet for their invaluable help, technical skills and/or fruitful discussions. The authors would like to thank P. de Mierry for critical reading of the manuscript and constructive remarks. P.V. and M. K. want to thank IMRA Europe S.A. for the access to the STEM JEOL 2100 microscope. This work is supported by the ANR Project <ANR-14-CE26-0025-01> "NANOGANUV". We acknowledge support from GANEX (ANR-11-LABX-0014). GANEX belongs to the publicly funded "Investissements d'Avenir" program managed by the French ANR agency.

[1] Kneissl M and Rass J 2016 III-Nitride Ultraviolet Emitters *Springer Series in Materials Science* 227
[2] Zhang J, Hu X, Lunev A, Deng J, Bilenko Y, Katona T M, Shur M S, Gaska R and Asif Khan M 2005 AlGaN Deep-Ultraviolet Light-Emitting Diodes *Jpn. J. Appl. Phys.* 44 7250
[3] Muramoto Y, Kimura M, and Nouda S 2014 Development and future of ultraviolet light-emitting diodes: UV-LED will replace the UV lamp *Semicond. Sci. Technol.* 29 084004
[4] Narukawa Y, Ichikawa M, Sanga D, Masahiko Sano M and Mukai T 2010 White light emitting diodes with super-high luminous efficacy *J. Phys. D: Appl. Phys.* 43 354002
[5] Ban K, Yamamoto J-i,Takeda K, Ide K, Iwaya M, Takeuchi T, Kamiyama S, Akasaki I and Amano H 2011 Internal Quantum Efficiency of Whole-Composition-Range AlGaN Multiquantum Wells *Appl. Phys. Express* 4 052101
[6] Cho Y H, Gainer G H, Fischer A J, Song J J, Keller S, Mishra U K and DenBaars S P 1998 "S-shaped" temperature-dependent emission shift and carrier dynamics in InGaN/GaN multiple quantum wells *Appl. Phys. Lett.* 73 1370-2
[7] Hirayama H, Fujikawa S, Norimatsu J, Takano T, Tsubaki K and Kamata N 2009 Fabrication of a low threading dislocation density ELO-AlN template for application to deep-UV LEDs *Phys. Status Solidi (c)* 6 S356–9
[8] Hagedorn S, Knauer A, Brunner F, Mogilatenko A, Zeimer U, Weyers M 2017 High-quality AlN grown on a thermally decomposed sapphire surface *Journal of Crystal Growth* 479 16-21
[9] Yoshikawa A, Nagatomi T, Morishita T, Iwaya M, Takeuchi T, Kamiyama S and Akasaki I 2017 High-quality AlN film grown on a nanosized concave–convex surface sapphire substrate by metalorganic vapor phase epitaxy *Appl. Phys. Lett.* 111 162102

[10] Miyake H, Nishio G, Suzuki S, Hiramatsu K, Fukuyama H, Kaur J and Kuwano N 2016 Annealing of an AlN buffer layer in N_2–CO for growth of a high-quality AlN film on sapphire *Appl. Phys. Express* 9 025501
[11] Nemoz M, Dagher R, Matta S, Michon A, Vennéguès P and Brault J 2017 Dislocation densities reduction in MBE-grown AlN thin films by high temperature annealing *J Crystal Growth* 461 10–5
[12] Bhattacharyya A, Moustakas T D, Zhou L, Smith D J and Hug W 2009 Deep ultraviolet emitting AlGaN quantum wells with high internal quantum efficiency *Appl. Phys. Lett.* 94 181907
[13] Borisov B, Nikishin S, Kuryatkov V and Temkin H 2005 Enhanced deep ultraviolet luminescence from AlGaN quantum wells grown in the three-dimensional mode *Appl. Phys. Lett.* 87 191902
[14] Daudin B, Widmann F, Feuillet G, Samson Y, Arlery M and Rouvière J L 1997 Stranski-Krastanov growth mode during the molecular beam epitaxy of highly strained GaN *Phys. Rev. B 56 R7069-72*
[15] Damilano B, Brault J, and Massies J 2015 Formation of GaN quantum dots by molecular beam epitaxy using NH_3 as nitrogen source *J. Appl. Phys.* 118 024304
[16] Renard J, Kandaswamy P K, Monroy E and Gayral B 2009 Suppression of nonradiative processes in long-lived polar GaN/AlN quantum dots *Appl. Phys. Lett.* 95 131903
[17] Himwas C, den Hertog M, Bellet-Amalric E, Songmuang R, Donatini F, Le Si Dang and Monroy E 2014 Enhanced room-temperature mid-ultraviolet emission from AlGaN/AlN Stranski-Krastanov quantum dots *J. Appl. Phys.* 116 023502
[18] Brault J, Matta S, Ngo T H, Korytov M, Rosales D, Damilano B, Leroux M, Vennéguès P, Al Khalfioui M, Courville A, Tottereau O, Massies J, and Gil B 2016 Investigation of $Al_yGa_{1-y}N/Al_{0.5}Ga_{0.5}N$ quantum dot properties for the design of ultraviolet emitters *Jpn. J. Appl. Phys.* 55 05FG06
[19] Matta S, Brault J, Ngo T H, Damilano B, Korytov M, Vennéguès P, Nemoz M, Massies J, Leroux M, and Gil B 2017 Influence of the heterostructure design on the optical properties of GaN and $Al_{0.1}Ga_{0.9}N$ quantum dots for ultraviolet emission *J. Appl. Phys.* 122 085706
[20] Tanaka S, Lee J S, Ramvall P and Okagawa H 2003 A UV Light-Emitting Diode Incorporating GaN Quantum Dots *Jpn. J. Appl. Phys.* 42 L885-3
[21] Liao Y, Thomidis C, Kao C K and Moustakas T D 2011 AlGaN based deep ultraviolet light emitting diodes with high internal quantum efficiency grown by molecular beam epitaxy *Appl. Phys. Lett.* 98 081110
[22] Verma J, Kandaswamy P K, Protasenko V, Verma A, Xing H G and Jena D 2013 Tunnel-injection GaN quantum dot ultraviolet light-emitting diodes *Appl. Phys. Lett.* 102 041103
[23] Huault T, Brault J, Natali F, Damilano B, Lefebvre D, Nguyen L, Leroux M and Massies J 2008 Blue-light emission from GaN / AlGa N quantum dots *Appl. Phys. Lett.* 92, 051911
[24] Brault J, Damilano B, Kahouli A, Chenot S, Leroux M, Vinter B and Massies J 2013 Ultra-violet $GaN/Al_{0.5}Ga_{0.5}N$ quantum dot based light emitting diodes *J Crystal Growth* 363 282–6
[25] Brault J, Damilano B, Vinter B, Vennéguès P, Leroux M, Kahouli A and Massies J 2013 AlGaN-Based Light Emitting Diodes Using Self-Assembled GaN Quantum Dots for Ultraviolet Emission *Jpn. J. Appl. Phys.* 52 08JG01
[26] Kahouli A, Kriouche N, Brault J, Damilano B, Vennéguès P, de Mierry P, Leroux M, Courville A, Tottereau O and Massies J 2011 $GaN/Al_{0.5}Ga_{0.5}N$ (11-22) semipolar nanostructures: A way to get high luminescence efficiency in the near ultraviolet range *J. Appl. Phys.* 110 084318

[27] Brault J, Matta S, Ngo T H, Rosales D, Leroux M, Damilano B, Al Khalfioui M, Tendille F, Chenot S, De Mierry P, Massies J and Gil B 2016 Ultraviolet light emitting diodes using III-N quantum dots *Mater. Sci. Semicond. Process.* 55, 95-101
[28] Brault J, Rosales D, Damilano B, Leroux M, Courville A, Korytov M, Chenot S, Vennéguès P, Vinter B, De Mierry P, Kahouli A, Massies J, Bretagnon T and Gil B 2014 Polar and semipolar GaN/$Al_{0.5}Ga_{0.5}N$ nanostructures for UV light emitters *Semicond. Sci. Technol.* 29 084001
[29] Korytov M, Benaissa M, Brault J, Huault T, Neisius T and Vennéguès P 2009 Effects of capping on GaN quantum dots deposited on $Al_{0.5}Ga_{0.5}N$ by molecular beam epitaxy *Appl. Phys. Lett.* 94 143105
[30] Korytov M, Budagosky J A, Brault J, Huault T, Rouvière J L and Vennéguès P 2012 Mechanism of GaN quantum dot overgrowth by $Al_{0.5}Ga_{0.5}N$: Strain evolution and phase separation *J. Appl. Phys.* 111 084309
[31] Leroux M, Brault J, Kahouli A, Maghraoui D, Damilano B, de Mierry P, Korytov M, Kim J H and Cho Y H 2014 Stark effect in ensembles of polar (0001) $Al_{0.5}Ga_{0.5}N$/GaN quantum dots and comparison with semipolar (11-22) ones *J. Appl. Phys.* 116 034308
[32] Lee S W, Oh D C, Goto H, Ha J S, Lee H J, Hanada T, Cho M W, Hong S K, Lee H Y, Cho S R, Choi J W, Choi J H, Jang J H, Shin J E and Lee J S 2006 Origin of forward leakage current in GaN-based light-emitting devices *Appl. Phys. Lett.* 89 132117
[33] Nepal N, Li J, Nakarmi M L, Lin J Y and Jiang H X 2005 Temperature and compositional dependence of the energy band gap of AlGaN alloys *Appl. Phys. Lett.* 87 242104
[34] Leroux M, Lahrèche H, Semond F, Laügt M, Feltin E, Schnell N, Beaumont B, Gibart P and Massies J 2001 From Relaxed to Highly Tensily Strained GaN Grown on 6H-SiC and Si(111): Optical Characterization *Mater Sci. Forum.* 353-356 795-8
[35] Bretagnon T, Lefebvre P, Valvin P, Bardoux R, Guillet T, Taliercio T, Gil B, Grandjean N, Semond F, Damilano B, Dussaigne A and Massies J 2006 Radiative lifetime of a single electron-hole pair in GaN⁄AlN quantum dots *Phys. Rev. B* 73 113304
[36] Matta S, Brault J, Ngo T H, Damilano B, Leroux M, Massies and Gil B 2017 Photoluminescence properties of (Al,Ga)N nanostructures grown on $Al_{0.5}Ga_{0.5}N$ (0001), *Superlattices and Microstructures* 114 161-8
[37] Stangl J, Holý V and Bauer G 2004 Structural properties of self-organized semiconductor nanostructures *Rev. Mod. Phys.* 76 725–76
[38] Brault J, Gendry M, Marty O, Pitaval M, Olivares J, Grenet G, Hollinger G 2000 Staggered vertical self-organization of stacked InAs/InAlAs quantum wires on InP (001) *Appl. Surf. Sci.* 162/163 584-9
[39] Dalmasso S , Damilano B, Pernot C, Dussaigne A, Byrne D, Grandjean N, Leroux M and Massies J 2002 Injection Dependence of the Electroluminescence Spectra of Phosphor Free GaN-Based White Light Emitting Diodes *phys. stat. sol. (a)* 192 139-43
[40] Cao X A, Topol K, Shahedipour-Sandvik F,Teetsov J, Sandvik P M, LeBoeuf S F, Ebong A, Kretchmer J, Stokes E B, Arthur S, Kaloyeros A E and Walker D 2002 Influence of defects on electrical and optical characteristics of GaN/InGaN-based light-emitting diodes *Proceedings of SPIE* 4776 105-13
[41] Hirayama H, Maeda N, Fujikawa S, Toyoda S and Kamata N 2014 Recent progress and future prospects of AlGaN-based high-efficiency deep-ultraviolet light-emitting diodes *Jpn. J. Appl. Phys.* 53 100209

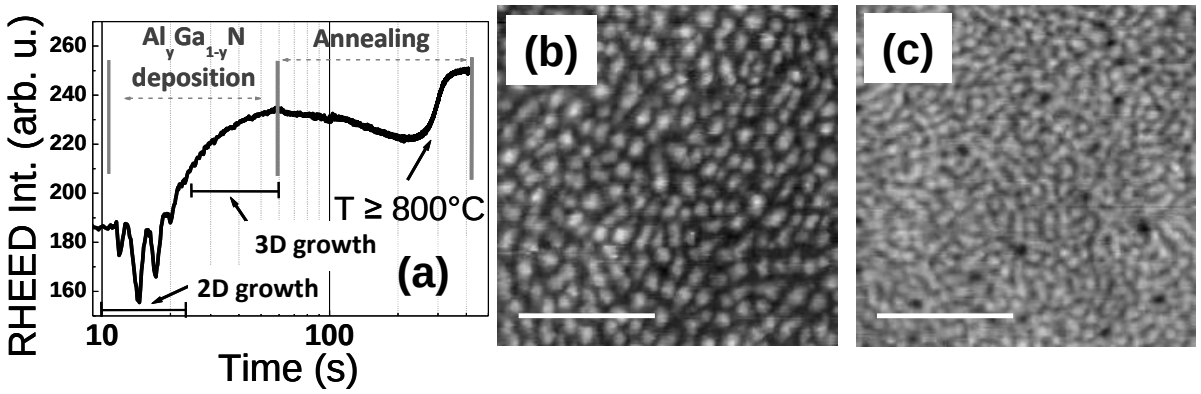

Figure 1. (a) Variation of the reflection high-energy electron diffraction intensity (RHEED) recorded during the formation of $Al_yGa_{1-y}N$ quantum dots (QDs). (b) and (c) Topographic AFM images of $Al_{0.1}Ga_{0.9}N$ and $Al_{0.2}Ga_{0.8}N$ QDs, respectively. The variation in height of both images corresponds to 4 nm and the white line indicates a lateral scale of 100 nm.

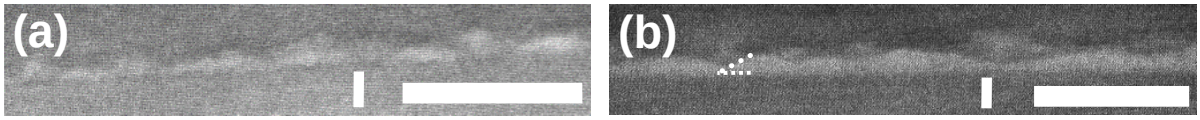

Figure 2. Cross-section high-angle annular dark-field imaging in scanning transmission electron microscopy mode of one QD plane (bright contrast) buried in an $Al_xGa_{1-x}N$ (0001) matrix (with x ~ 0.6) for a QD nominal composition of: a) $Al_{0.1}Ga_{0.9}N$ and b) $Al_{0.2}Ga_{0.8}N$. The thick horizontal white line and the thin vertical one in (a) and (b) represent a scale of 20 nm and 4 nm, respectively.. The angle formed by the dotted segments between a facet and the base of a QD in figure (b) is found to be ~ 30°.

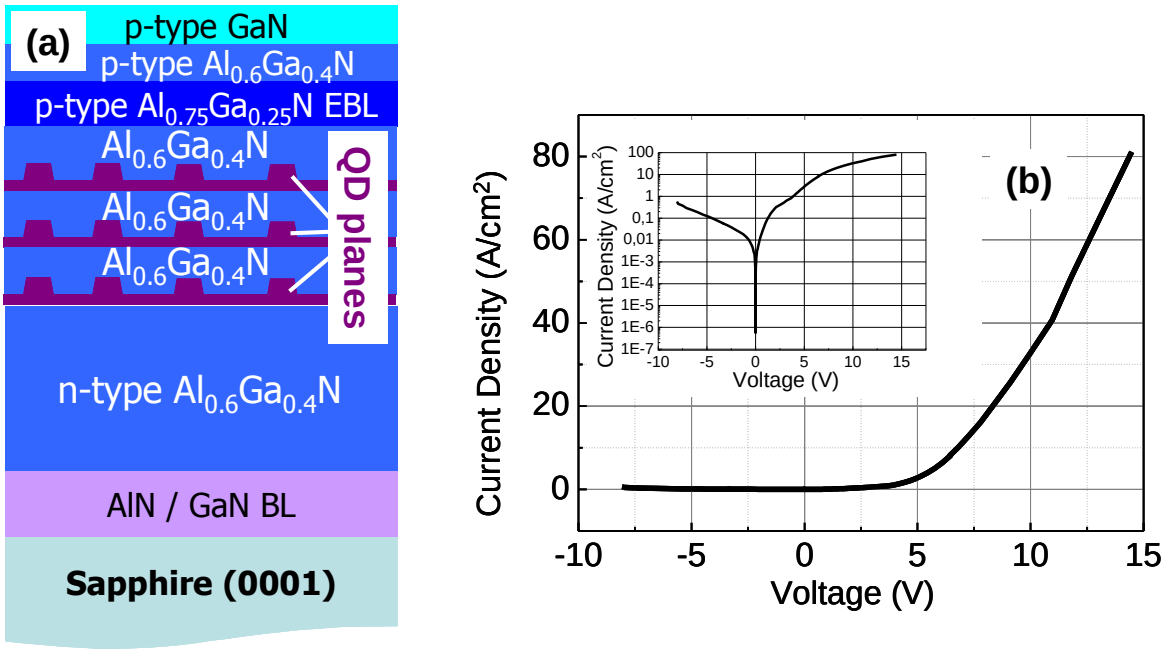

Figure 3. (a) Epitaxial structure of the light emitting diodes using $Al_yGa_{1-y}N/Al_{0.6}Ga_{0.4}N$ quantum dots (with y = 0.1 or 0.2) active regions. (b) Representative Current –Voltage characteristic of an $Al_yGa_{1-y}N/Al_{0.6}Ga_{0.4}N$ quantum dot based UV light emitting diode (log scale in insert).

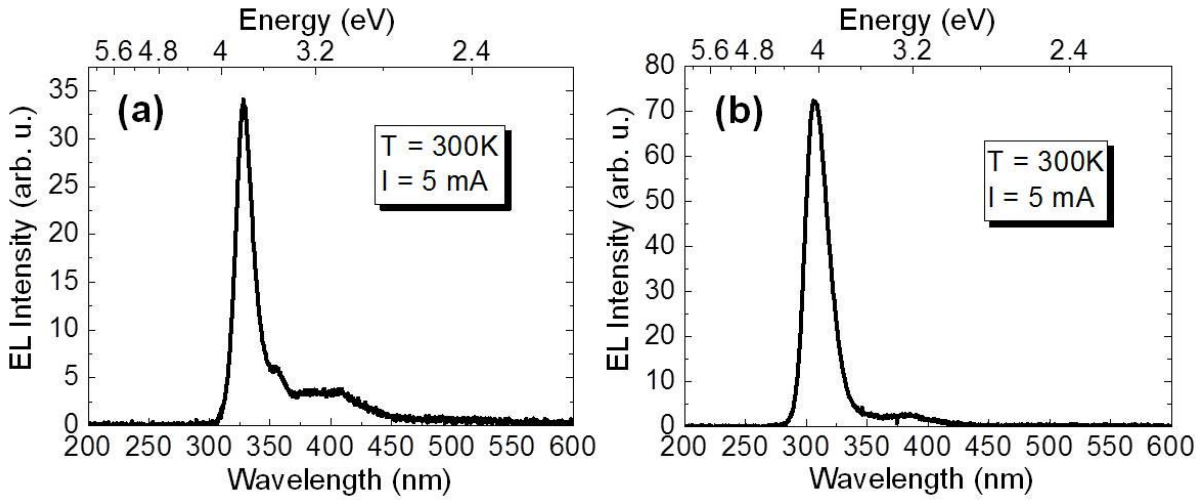

Figure 4. Electroluminescence spectra over a broad spectral range of $A_{ly}Ga_{1-y}N/Al_{0.6}Ga_{0.4}N$ QD-based LEDs for an injection current of 5 mA (i.e. a current density of ~ 5.7 A/cm^2) with: (a) $Al_{0.1}Ga_{0.9}N$ (A1) and (b) $Al_{0.2}Ga_{0.8}N$ QD (B1) active regions. Each spectrum is characterized by a main peak, coming from the QD emission, found at an energy of 3.81 eV (325 nm) for A1 and at an energy of 4.06 eV (305 nm) for B1. The EL peaks full width at half maximum have a value of 190 meV (16 nm) for A1 and a value of 280 meV (22 nm) for B1.

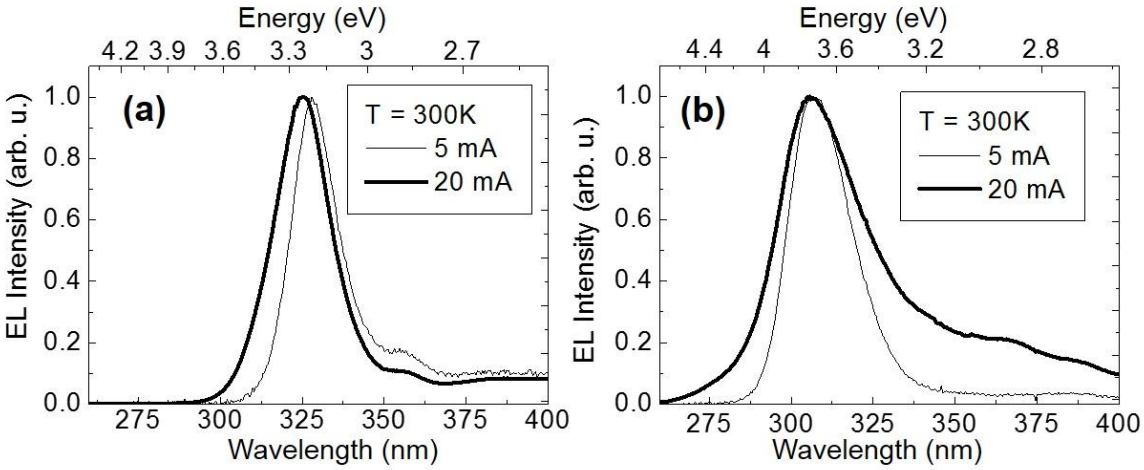

Figure 5. Normalized electroluminescence (EL) spectra of $Al_yGa_{1-y}N/Al_{0.6}Ga_{0.4}N$ QD-based LEDs for injection currents of 5 mA and 20 mA (i.e. current densities of ~ 5.7 A/cm^2 and ~ 23 A/cm^2) with: (a) $Al_{0.1}Ga_{0.9}N$ (A1) and (b) $Al_{0.2}Ga_{0.8}N$ (B1) QD active regions. At 20 mA, the EL spectra are found at an energy of 3.80 eV (326 nm) for A1 and at an energy of 4.06 eV (305 nm) for B1. The EL peaks full width at half maximum have a value of 190 meV (16 nm) and 230 meV (20 nm) for A1 and of 280 meV (22 nm) and 425 meV (32 nm) for B1, for injection currents of 5 mA and 20 mA, respectively.

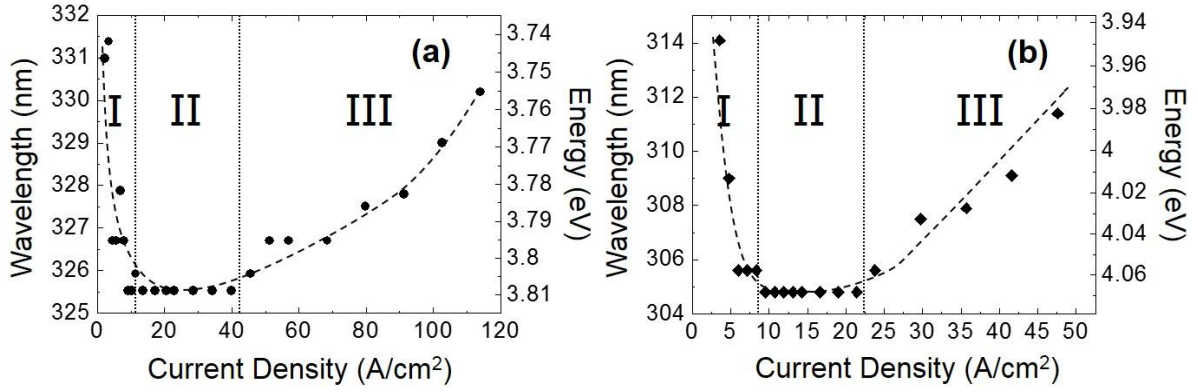

Figure 6. Variation of the wavelength emission of $Al_yGa_{1-y}N/Al_{0.6}Ga_{0.4}N$ QD-based LEDs as a function of the injection current density for (a) $Al_{0.1}Ga_{0.9}N$ (full dots) and (b) $Al_{0.2}Ga_{0.8}N$ QD (diamonds) active regions. The dashed curves are guides for the eyes.

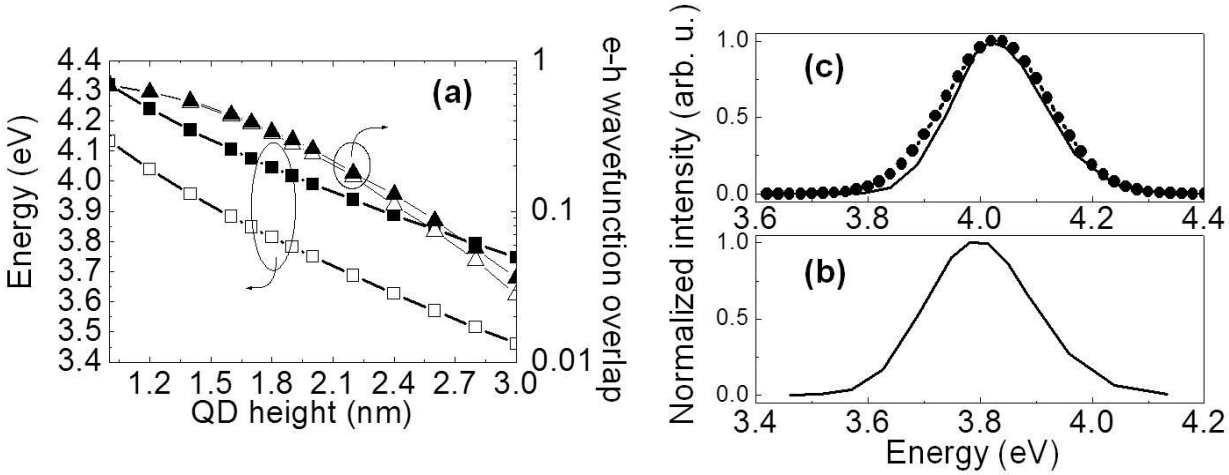

Figure 7. (a) Calculated emission energy (squares) and electron-hole wave function overlap (triangles) for $Al_yGa_{1-y}N$ / $Al_{0.6}Ga_{0.4}N$ QDs with y equals 0.1 (empty symbols) and 0.2 (full symbols), as a function of the QD height. (right) Calculated emission spectrum for $Al_yGa_{1-y}N$ / $Al_{0.6}Ga_{0.4}N$ QDs with y equals 0.1 (b) and 0.2 (c), considering a Gaussian population of QDs with a mean height of 2nm and a Gaussian parameter of 0.3 nm. The resulting emission properties (mean energy and FWHM) are shown in the figure (full lines). The full circles represented in (c) characterize the calculated emission spectrum (mean energy and FWHM) for $Al_{0.2}Ga_{0.8}N$ / $Al_{0.6}Ga_{0.4}N$ QDs considering an identical Gaussian population distribution of QDs and adding a Gaussian Al composition fluctuation with a mean Al value of 20% and a Gaussian parameter of 2%.

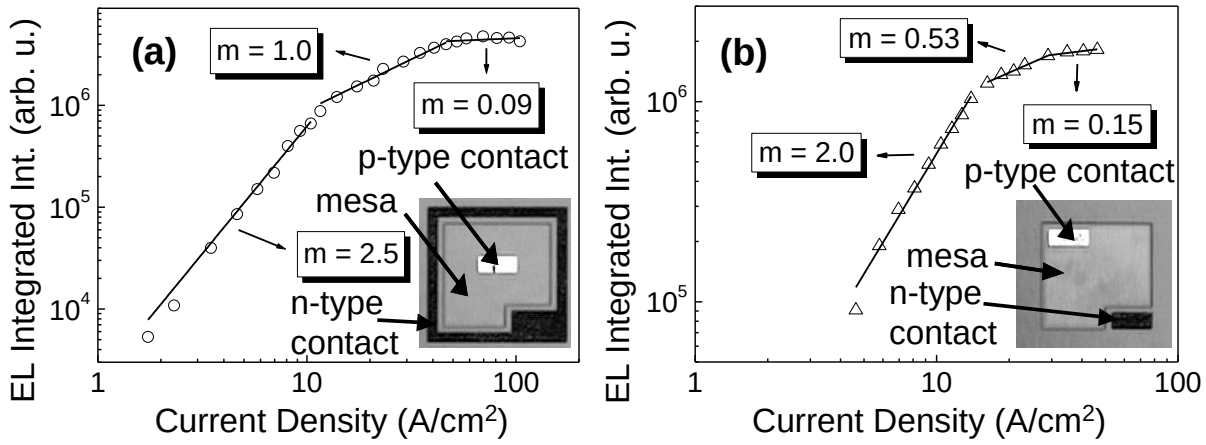

Figure 8. Variation of the light output (i.e. integrated electroluminescence efficiency) of $Al_yGa_{1-y}N/Al_{0.6}Ga_{0.4}N$ QD-based LEDs as a function of the injection current density for different LED designs: (a) an n-type contact surrounding the entire mesa and (b) an n-type contact at the right-side edge of the mesa (represented by the darker area in each photograph inserted in the figures).